inorganics

MDPI

Article

Direct Z-Scheme $CoFe_2O_4$-Loaded g-C_3N_4 Photocatalyst with High Degradation Efficiency of Methylene Blue under Visible-Light Irradiation

Gebrehiwot Gebreslassie [1,2,*], Mamo Gebrezgiabher [1,2], Bin Lin [3], Madhu Thomas [1,2] and Wolfgang Linert [4,*]

1 Department of Industrial Chemistry, Addis Ababa Science and Technology University, Addis Ababa 16417, Ethiopia; mamo.gebrezgiabher@aastu.edu.et (M.G.); madhu.thomas@aastu.edu.et (M.T.)
2 Nanotechnology Center of Excellence, Addis Ababa Science and Technology University, Addis Ababa 16417, Ethiopia
3 School of Mechanical and Electrical Engineering, University of Electronic Science and Technology of China, Chengdu 611731, China; bin@uestc.edu.cn
4 Institute of Applied Physics, Vienna University of Technology, Wiedner Hauptstraße 8-10, 1040 Vienna, Austria
* Correspondence: gebrehiwot.gebreslassie@aastu.edu.et (G.G.); wolfgang.linert@tuwien.ac.at (W.L.); Tel.: +251-1246-7711 (G.G.); +43-1-58801-163613 (W.L.)

Abstract: Magnetically recyclable direct Z-scheme $CoFe_2O_4$-loaded g-C_3N_4 photocatalyst material was fabricated using a facile hydrothermal technique and subsequently characterized by XRD, VSM, PL, FT-IR, EDX, DRS, SEM, and BET techniques. The characterization results confirmed that nanoparticles of $CoFe_2O_4$ are loaded on the surface of g-C_3N_4 sheets. The optical band gap of g-C_3N_4 has been decreased from 2.65 eV to 1.30 eV by means of the loading of $CoFe_2O_4$ nanoparticles onto the nanosheets of g-C_3N_4. This has enhanced the separation process of electron-hole. Under visible light irradiation, the photocatalytic activity of the developed direct Z-scheme $CoFe_2O_4$-loaded g-C_3N_4 photocatalyst was evaluated for the photodegradation of methylene blue (MB); during this process the MB decomposed by up to 98.86% in 140 min. Meanwhile, under the same irradiation and time conditions, the g-C_3N_4 and $CoFe_2O_4$ themselves degraded MB up to 74.92% and 51.53%, respectively. The direct Z-scheme $CoFe_2O_4$-loaded g-C_3N_4 material was recovered from the solution after the photocatalytic activity using an external magnet and studied to determine its stability. It was shown that the photoactivity did not change significantly after five consecutive cycles.

Keywords: direct Z-scheme photocatalyst; $CoFe_2O_4$; graphitic carbon nitride; dye degradation

check for updates

Citation: Gebreslassie, G.; Gebrezgiabher, M.; Lin, B.; Thomas, M.; Linert, W. Direct Z-Scheme $CoFe_2O_4$-Loaded g-C_3N_4 Photocatalyst with High Degradation Efficiency of Methylene Blue under Visible-Light Irradiation. *Inorganics* **2023**, *11*, 119. https://doi.org/10.3390/inorganics11030119

Academic Editor: Antonino Gulino

Received: 15 February 2023
Revised: 7 March 2023
Accepted: 11 March 2023
Published: 13 March 2023

1. Introduction

With the increasing expansion of global industry, the problem of access to clean water has risen to the forefront of discussion. Every year, a massive volume of industrial dye wastewater is dumped into natural water bodies, posing a risk to both the aquatic ecosystem and people [1]. Nowadays, removal of organic pollutants from wastewater/water through photocatalysis provides a viable method for solving environmental issues [2,3]. In order to eliminate environmental pollution and degrade these harmful organic pollutants, photocatalytic technology has received an increasing amount of interest. So far, TiO_2 is the most widely studied photocatalyst; it was reported by Fujishima and Honda in 1972 for use in photoelectrochemical water splitting [4]. This study was a pioneer in photocatalysis technology. Nevertheless, TiO_2 has high band gap (3.2 eV), which accounts for around 4% of sunlight; this severely restricts its ability to function as a photocatalyst and restricts the range of use of this material [5,6]. These limitations have inspired researchers to develop novel materials with narrow band gaps (E_g) to utilize solar energy in a more efficient way. Due to its chemical inertness, distinctive layered structure, nontoxic nature, a middle band

(i.e., band gap between 2.4–2.9 eV), and capacity to absorb visible light, graphitic carbon nitride (g-C_3N_4) is now frequently employed for the photocatalytic degradation of organic contaminants [7–14]. However, inadequate absorption of visible light, small specific surface area, and fast electron-hole pair recombination still limits its photocatalytic activity [15,16].

Thus, numerous techniques were exploited to improve graphitic carbon nitride's photocatalytic efficiency, including doping [12], morphological modification [17], copolymerization [18], and combining with one or more semiconductor materials [19]. Thanks to its appropriate valence band edge and conduction band edge positions, g-C_3N_4 can produce a heterojunction structure/nanocomposite with other semiconductor photocatalysts. This could improve its photocatalytic activity performance by improving the photogenerated electron-hole separation rate of the heterojunction photocatalyst [20–22]. Currently, spinel ferrites with the general formula of MFe_2O_4 (M = Zn, Co, Ni, Cu) have been widely used in photocatalytic applications due to their visible-light absorption, stability, environmentally friendly nature, magnetic properties, and low-cost [23]. Cobalt ferrite ($CoFe_2O_4$) is one of the inverse spinel structures that attracted significant interest because of its non-toxic nature and its abundant and narrow bandgap (1.2–2.7 eV) [24,25]. Even though pristine $CoFe_2O_4$ has a poor photocatalytic performance, its photocatalytic activity considerably increases when it is coupled with a π-conjugated semiconductor materials [26]. For instance, $CoFe_2O_4$ nanoparticles can be coupled with g-C_3N_4 to prepare heterojunction structures, direct Z-schemes, or all-solid-state Z-schemes due to the matching conduction band edge position and valence band edge position of $CoFe_2O_4$ and g-C_3N_4 semiconductors.

Huang et al. [27] reported on the $CoFe_2O_4$/g-C_3N_4 composites, which are synthesized using an easy calcination process. The composite containing 41.4 wt% $CoFe_2O_4$ showed the maximum catalytic activity for the MB degradation under irradiation of visible light in the presence of H_2O_2. However, the use of H_2O_2 may not be economically viable during practical applications. Inbaraj et al. [28] also synthesized $CoFe_2O_4$/g-C_3N_4 composite via the coupling of a honey-mediated green approach and hydrothermal technique. The MB degradation and the adsorption removal of lead (Pb^{2+}) ion from water were both used to test the photocatalytic activity of the composite photocatalyst. However, the hydrothermal process used in the synthesis is time-consuming and labor-intensive; our experimental strategy seems to be simpler. Moreover, the photocatalytic mechanism was a type-II heterojunction, which means the redox reaction takes place in the less negative conduction band/reduction potential and in the less positive valence band/oxidation potential of the semiconductors. This limits the photocatalytic performance of the $CoFe_2O_4$/g-C_3N_4 composites. Recently, in the presence of peroxymonosulfate (PMS), which is utilized as a sulfate radical-based Fenton-like oxidation reaction, Guo et al. [1] reported that rhodamine B (RhB) was photodegraded by $CoFe_2O_4$@g-C_3N_4 photocatalyst material. The Fen+/PMS system must be run at an acidic pH because of the precipitation and hydrolysis of iron ions; doing so after the reaction results in additional operational costs [29,30]. These inescapable disadvantages limit the widespread application of the homogeneous iron/PMS approach in wastewater treatment technology.

Even though several research have been widely published about the photocatalytic activity of the $CoFe_2O_4$/g-C_3N_4 composite and its ability to photodegrade several organic dyes/pollutants, the literature currently available falls significantly short in addressing crucial variables, including (1) construction of the direct Z-scheme structure and (2) the photoactivity of the composite in the absence of a Fenton-like system. Hence, to overcome these challenges, direct Z-scheme $CoFe_2O_4$-loaded g-C_3N_4 photocatalyst material was successfully fabricated using the facile hydrothermal method.

The photodegradation activity of the obtained direct Z-scheme $CoFe_2O_4$-loaded g-C_3N_4 photocatalyst was assessed for methylene blue (MB) photodegradation under irradiation of visible light and shows degradation activity 6.6 and 3.6 times higher than pristine $CoFe_2O_4$ and pure g-C_3N_4 photocatalysts, respectively. Such an extraordinary enhancement of catalytic activity under irradiation of visible-light could be due to the significantly increased electron-hole separation in the direct Z-scheme g-$CoFe_2O_4$-loaded

g-C_3N_4, which improves the oxidation/reduction ability of the photocatalytic reaction. Moreover, the direct Z-scheme g-$CoFe_2O_4$-loaded g-C_3N_4 photocatalyst was collected from the aqueous solution without significant loss and demonstrated a negligible decline in performance throughout five cycles.

2. Results and Discussion

2.1. Characterization of the Photocatalyst

The FT-IR spectra of $CoFe_2O_4$, g-C_3N_4, and $CoFe_2O_4$-loaded g-C_3N_4 are displayed in Figure 1. As shown in Figure 1a, the broad bands in the 3086–3252 cm^{-1} matches to the -NH stretching mode at the uncondensed sites of the aromatic structures [31]. The peaks at 1572 and 1639 cm^{-1}, and the other four peaks at 1407, 1461, 1316, and 1236 cm^{-1}, represented typical C=N stretching vibration modes and C-N stretching of g-C_3N_4, respectively. The intense peak at 812 cm^{-1} can be attributed to the tri-s-triazine units' breathing mode [7,32,33]. In spectrum of $CoFe_2O_4$, in the range of 587 and 419 cm^{-1}, there were two prominent absorption bands that are ascribed to both the tetrahedral and octahedral metal-oxygen (M-O) vibrational modes links in the spinel lattice of $CoFe_2O_4$ nanoparticles, as shown in Figure 1b [34]. The H-O-H bending vibration of absorbed or free water molecules is responsible for the peak seen at 3408 cm^{-1}. All the important characteristic peaks of $CoFe_2O_4$ and g-C_3N_4 appeared in the $CoFe_2O_4$-loaded g-C_3N_4 material; this confirmed the formation of $CoFe_2O_4$-loaded g-C_3N_4 photocatalyst material (Figure 1c).

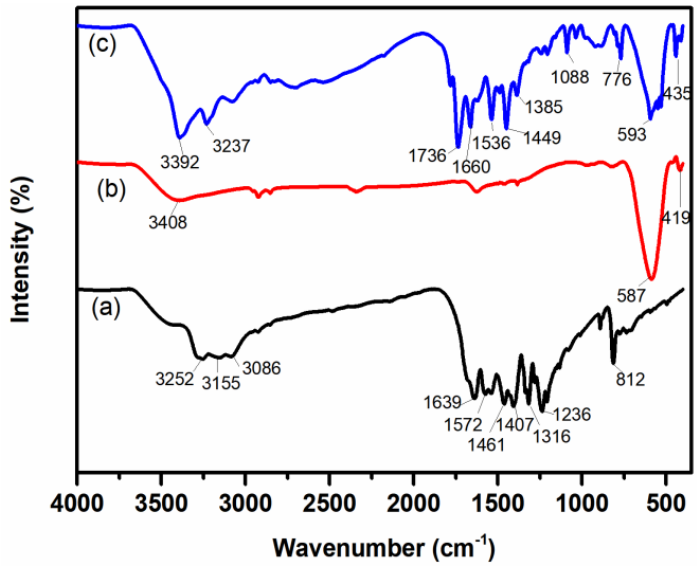

Figure 1. FTIR spectra of (**a**) g-C_3N_4, (**b**) $CoFe_2O_4$, (**c**) $CoFe_2O_4$-loaded g-C_3N_4 photocatalysts.

XRD spectra of all the photocatalysts were taken for phase identification. Figure 2 displays the XRD spectra of $CoFe_2O_4$, g-C_3N_4, and $CoFe_2O_4$-loaded g-C_3N_4 photocatalysts. The diffraction peaks at 30°, 35.62°, 43.28°, 53.78°, 57°, and 62.27° are willingly attributed to the face centered cubic inverse spinel crystal structure of $CoFe_2O_4$ (JCPDS file no: 22-1086) [35]. The XRD spectrum from pure g-C_3N_4 exhibited peaks at 27.52° and 12.74°; these can be assigned to the (002) and (100) crystal planes of polymeric g-C_3N_4, respectively. In the spectrum of the $CoFe_2O_4$-loaded g-C_3N_4, all diffraction peaks of g-C_3N_4 and $CoFe_2O_4$ are observed, indicating that the $CoFe_2O_4$-loaded g-C_3N_4 photocatalyst materials were successfully prepared. Moreover, the Scherrer's formula was used to determine the average crystallite size of $CoFe_2O_4$-loaded g-C_3N_4 photocatalyst and [36,37]; this was determined to be 13.43 nm.

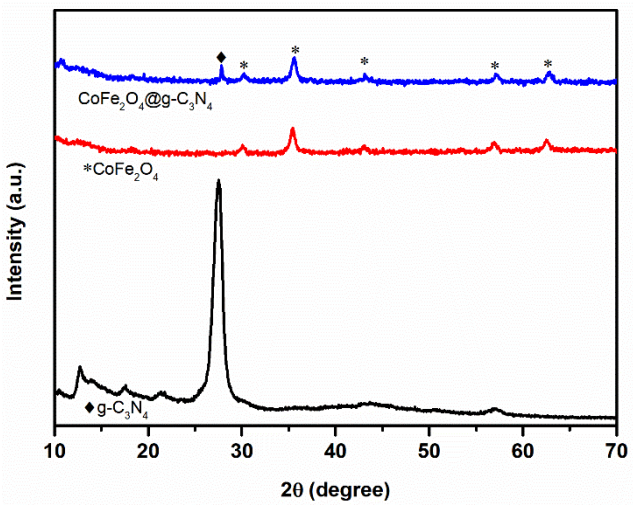

Figure 2. XRD patterns of g-C_3N_4, $CoFe_2O_4$, and $CoFe_2O_4$-loaded g-C_3N_4 photocatalyst.

The surface morphology and texture of the photocatalysts were investigated using SEM; the image is presented Figure 3a–c. The cubic structure of $CoFe_2O_4$ and crumpled sheets g-C_3N_4 are observed in Figure 3a,b, respectively. It has also been observed that numerous nanoparticles of $CoFe_2O_4$ were loaded on the g-C_3N_4 sheet surface (Figure 3c), suggesting the formation of $CoFe_2O_4$-loaded g-C_3N_4 photocatalyst. The elemental composition of the fabricated samples was examined using EDX; the spectra is displayed in Figure 3d–f. As shown in Figure 3a, the EDX peaks of the pristine $CoFe_2O_4$ sample are accredited to the elements Fe, Co, and O. The peaks in the EDX of neat g-C_3N_4 are linked to the elements C and N, as shown in Figure 3e. Also, the equivalent EDX spectrum of g-C_3N_4 that has $CoFe_2O_4$ loaded on it exhibits the presence of C, N, Co, Fe, and O, as shown in Figure 3f. This confirms the $CoFe_2O_4$-loaded g-C_3N_4 photocatalyst was synthesized without any additional impurities.

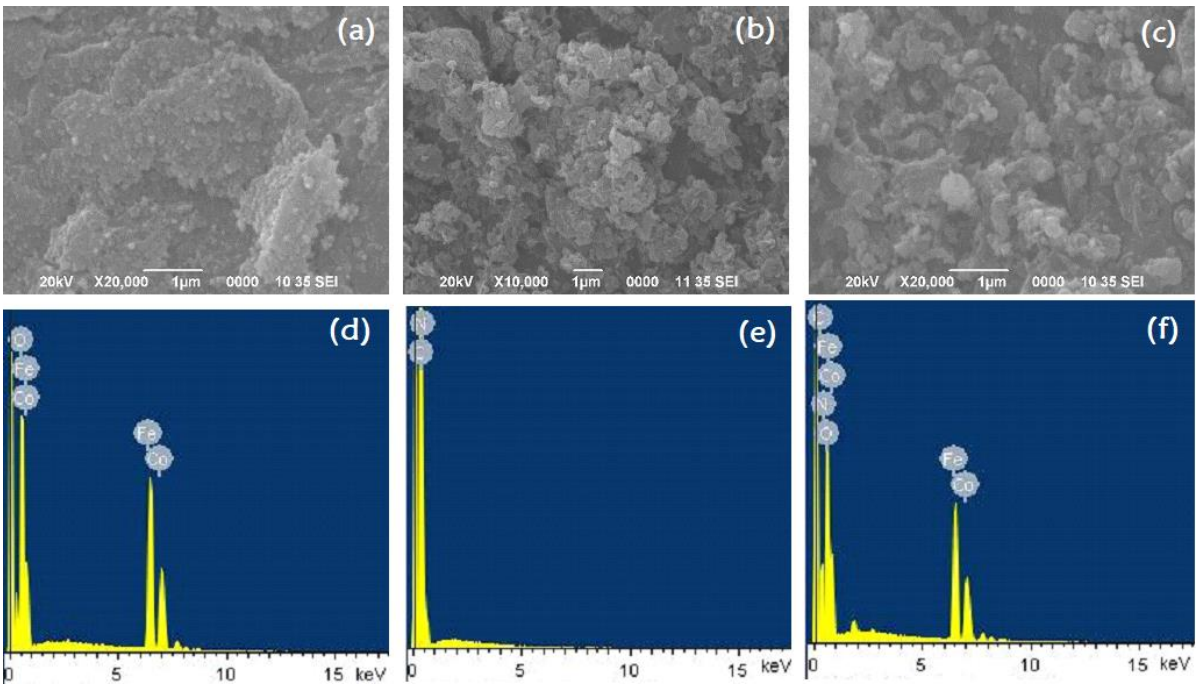

Figure 3. SEM images of (**a**) pure $CoFe_2O_4$, (**b**) pure g-C_3N_4, and (**c**) $CoFe_2O_4$-loaded g-C_3N_4 photocatalyst, and EDX pattern of (**d**) pure $CoFe_2O_4$, (**e**) pure g-C_3N_4, and (**f**) $CoFe_2O_4$-loaded g-C_3N_4 photocatalyst.

The magnetic possessions of the $CoFe_2O_4$-loaded g-C_3N_4 material and pristine $CoFe_2O_4$ photocatalysts were studied; the magnetization hysteresis curves are shown in Figure 4. The saturation magnetization (Ms) of pristine $CoFe_2O_4$ and $CoFe_2O_4$-loaded g-C_3N_4 photocatalyst was determined to be 43.4 emu/g and 41.9 emu/g, respectively. As a result, the $CoFe_2O_4$-loaded g-C_3N_4 photocatalyst could be easily collected using a magnet.

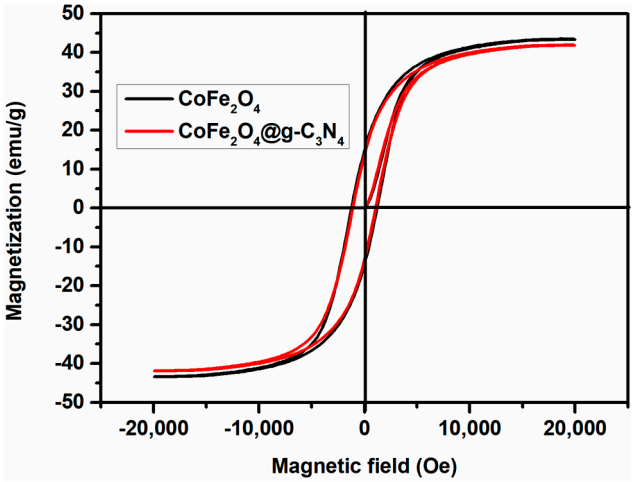

Figure 4. The magnetic hysteresis loops of pure $CoFe_2O_4$ and $CoFe_2O_4$-loaded g-C_3N_4 photocatalyst material.

The pore size distribution, surface area, and pore volume of the $CoFe_2O_4$-loaded g-C_3N_4 photocatalyst were studied using N_2 adsorption and desorption isotherms. The type IV isotherm and H3 hysteresis loop of the N_2 adsorption-desorption curve are clearly visible in Figure 5a, confirming the mesoporous nature of the $CoFe_2O_4$-loaded gC_3N_4 photocatalyst [38]. The Barrett–Joyner–Halenda equation and Brunauer–Emmett–Teller (BET) method were used to determine the photocatalyst's pore size distribution and surface area. The BET specific surface area of $CoFe_2O_4$-loaded g-C_3N_4 photocatalyst was determined to be 63.632 m^2/g. Furthermore, the pore volume and pore size of the $CoFe_2O_4$-loaded g-C_3N_4 photocatalyst was 4.29 nm and 0.247 cm^3/g, respectively, as presented as Figure 5b.

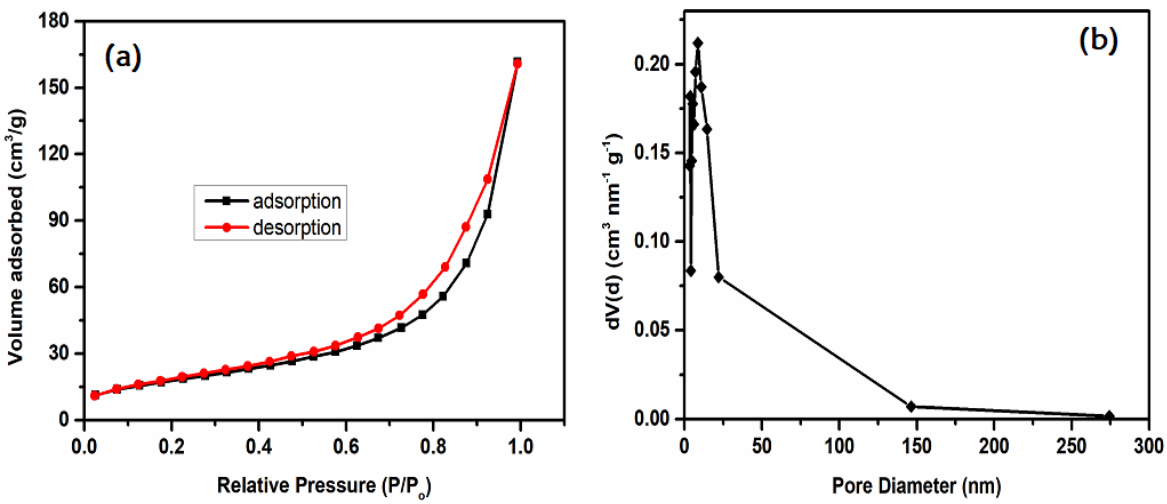

Figure 5. (**a**) N_2 adsorption–desorption isotherm of $CoFe_2O_4$-loaded g-C_3N_4 photocatalyst, and (**b**) the pore size distribution curve of $CoFe_2O_4$-loaded g-C_3N_4 photocatalyst.

The UV−vis DRS spectra of g-C_3N_4, $CoFe_2O_4$, and $CoFe_2O_4$-loaded g-C_3N_4 samples are shown in Figure 6a. The pristine g-C_3N_4 photocatalyst possessed an absorption edge at about 500 nm. The $CoFe_2O_4$ nanoparticle showed a wide absorption range (200 to 900 nm).

The absorption efficiency of the g-C_3N_4 photocatalyst was significantly extended in the visible-light region after loading nanoparticles of $CoFe_2O_4$ onto the g-C_3N_4 (Figure 6a). As a result, the boosted visible light absorption of the $CoFe_2O_4$-loaded g-C_3N_4 led to the production of extra electron−hole pairs under irradiation of visible-light, which boosted its photocatalytic activity. Furthermore, the band gap energy (E_g) of the photocatalysts were assessed using Tauc's equation and the results are displayed in Figure 6b,c. The obtained band gap (E_g) values for pristine $CoFe_2O_4$ and g-C_3N_4 are 1.30 eV and 2.65 eV, respectively. However, after loading the $CoFe_2O_4$ on the surface of g-C_3N_4 nanosheets, its band gap energy (E_g) decreased to 1.42 eV. This result confirmed that the visible light absorption efficiency of g-C_3N_4 was significantly improved after modification by $CoFe_2O_4$ nanoparticles.

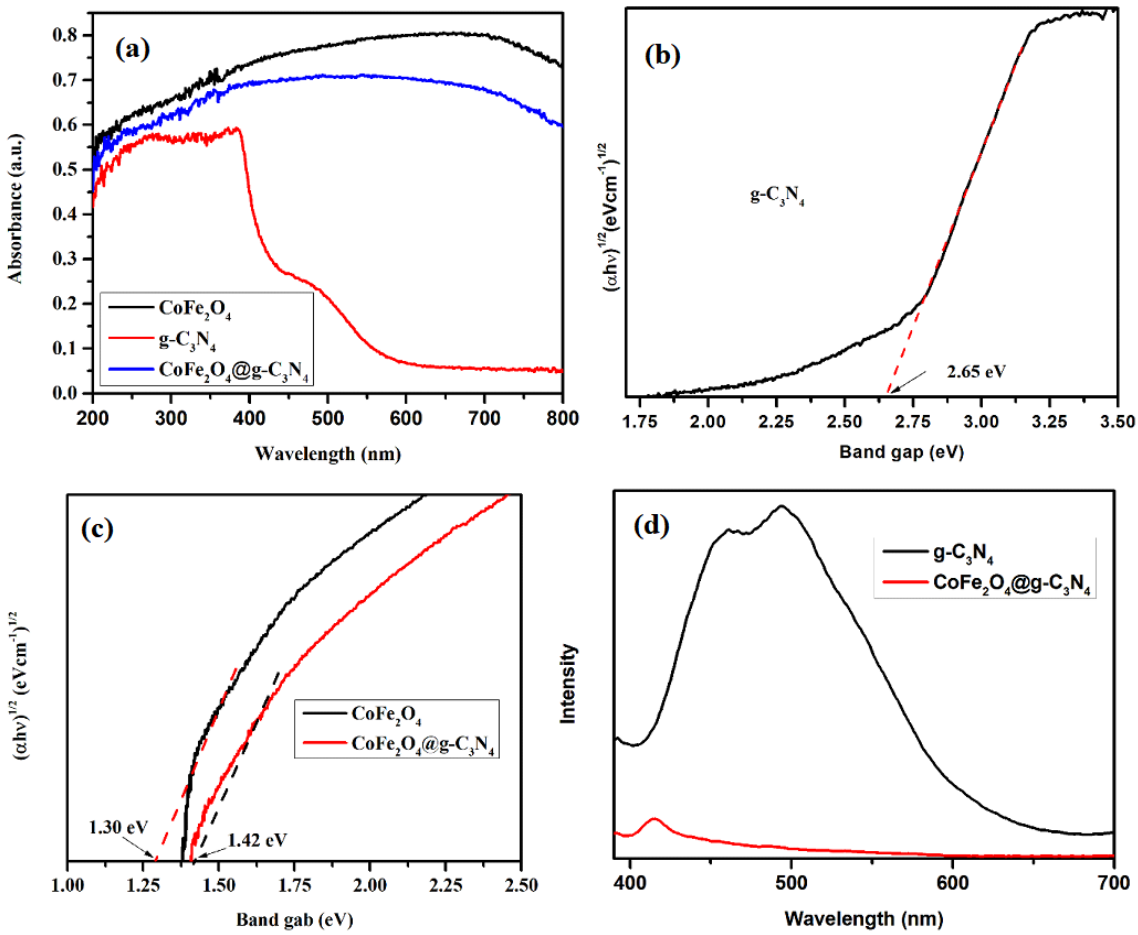

Figure 6. (**a**) DRS spectra of g-C_3N_4, $CoFe_2O_4$, and $CoFe_2O_4$-loaded g-C_3N_4 photocatalyst. (**b**) Tauc plot for g-C_3N_4 photocatalyst. (**c**) Tauc plot for $CoFe_2O_4$ and $CoFe_2O_4$-loaded g-C_3N_4 photocatalyst. (**d**) PL spectra of g-C_3N_4, and $CoFe_2O_4$-loaded g-C_3N_4 photocatalyst.

The photogenerated produced electron-hole pairs separation efficiency of the g-C_3N_4 and $CoFe_2O_4$-loaded g-C_3N_4 photocatalysts was examined using PL; the result is presented in Figure 6d. The PL strength of the $CoFe_2O_4$-loaded g-C_3N_4 is enormously diminished when compared to that of the pristine g-C_3N_4. This result shows that the rate of electron-hole separation efficiency in the $CoFe_2O_4$-loaded g-C_3N_4 was better than that in the g-C_3N_4 material. This could be because of the transfer of the electron-hole pairs between $CoFe_2O_4$ and g-C_3N_4 in the $CoFe_2O_4$-loaded g-C_3N_4.

2.2. Photocatalytic Activity

Figure 7a depicts the MB degradation under irradiation of visible light without photocatalyst as well as with $CoFe_2O_4$, g-C_3N_4, and $CoFe_2O_4$-loaded g-C_3N_4 photocatalysts.

Figure 7a demonstrates that, without a photocatalyst, the MB is practically stable for 140 min when irradiated using visible light. This demonstrates that the presence of a photocatalyst caused MB degradation. The $CoFe_2O_4$-loaded g-C_3N_4 photocatalyst degraded 98.86% of the MB within 140 min under irradiation of visible light. However, under the same irradiation and time conditions, the g-C_3N_4 and $CoFe_2O_4$ degraded MB up to 74.92% and 51.53%, respectively. Therefore, the photodegradation rates of MB by the $CoFe_2O_4$-loaded g-C_3N_4 photocatalyst was better than that of pure $CoFe_2O_4$ and pristine g-C_3N_4 photocatalysts. In addition, the rate constant (k_{ap}) of degradation of MB by the $CoFe_2O_4$, g-C_3N_4, and $CoFe_2O_4$-loaded g-C_3N_4 photocatalysts can be expressed by a pseudo-first-order kinetics equation: $\ln(C_o/C) = k_{ap}t$, where C_o is initial concentration, C is concentration after irradiation at a time t, and k_{ap} is apparent pseudo-first-order rate constant (Figure 7b). As shown in Figure 7b, the k_{ap} of g-C_3N_4 is higher than that of $CoFe_2O_4$. However, after loading $CoFe_2O_4$ on the g-C_3N_4 sheets surface, its k_{ap} increased significantly. As a result, $CoFe_2O_4$-loaded g-C_3N_4 photocatalysts showed photodegradation activity with 6.6 and 3.6 times higher k_{ap} than pristine $CoFe_2O_4$ and g-C_3N_4, respectively. This might be a result of the components' synergistic interaction. Table 1 compares the degradation efficiency of different materials from the literature with the fabricated direct Z-scheme $CoFe_2O_4$-loaded g-C_3N_4 photocatalyst material for the photodegradation of organic dyes in water.

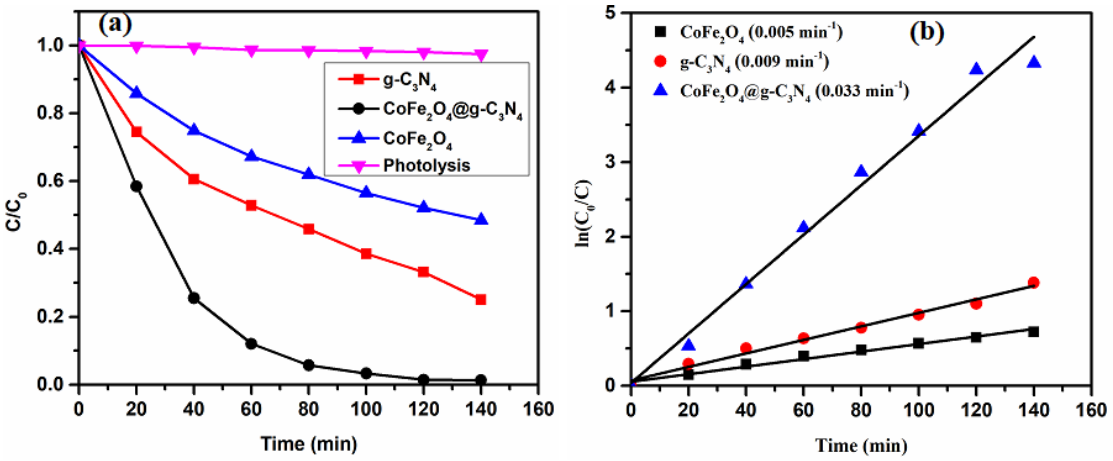

Figure 7. (**a**) Photodegradation of MB by $CoFe_2O_4$, g-C_3N_4, and $CoFe_2O_4$-loaded g-C_3N_4 photocatalysts under visible light irradiation. (**b**) Photodegradation rate constant (k_{ap}) of MB over the $CoFe_2O_4$, g-C_3N_4, and $CoFe_2O_4$-loaded g-C_3N_4 photocatalysts.

Table 1. Comparison of the effectiveness of several magnetic photocatalysts in the degradation of organic dyes.

No.	Photocatalyst	Light Source	Target Dye	Degradation Efficiency	Ref.
1	$CoFe_2O_4$/g-C_3N_4	Sun light	MB	98%/150 min	[28]
2	41.4% $CoFe_2O_4$/g-C_3N_4-H_2O_2	Xenon lamp	MB	97.3%/180 min	[27]
3	$CoFe_2O_4$/g-C_3N_4-PMS	Halogen tungsten lamp	RhB	96%/30 min	[1]
4	Direct Z-scheme $CoFe_2O_4$-loaded g-C_3N_4	LED lamp	MB	98.86%/140 min	This work

The stability of $CoFe_2O_4$-loaded g-C_3N_4 photocatalyst was examined by recycling and using it for repeated photocatalytic reactions. The $CoFe_2O_4$-loaded g-C_3N_4 photocatalyst exhibits nearly the same photocatalytic activity after five consecutive cycles of the degradation reaction, as displayed in Figure 8, demonstrating the produced photocatalyst's exceptional stability. This could be due to the good adherence of the $CoFe_2O_4$ nanoparticles on the g-C_3N_4 sheets.

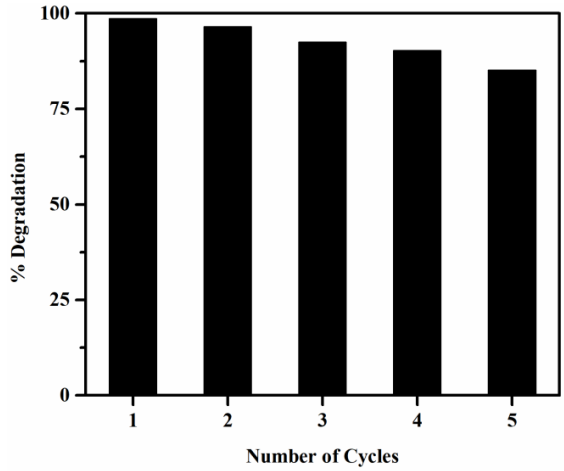

Figure 8. Reusability of the $CoFe_2O_4$-loaded g-C_3N_4 photocatalyst after five successive runs.

In order to explore the principal active species in the photocatalytic process, reactive species detection tests were also conducted. As superoxide radical (•O_2), hydroxyl radical (•OH), and hole (h^+) scavengers, p-benzoquinone (BQ), isopropanol (IPA), and formic acid (FA) were introduced at the same concentration (0.5 mmol/L), respectively [39,40]. As shown in Figure 9, the addition of IPA has an insignificant effect on the degradation efficiency, while the addition of BQ and FA diminished the degradation efficiency to 37.8% and 62.54%, respectively. Therefore, •O_2^- and h^+ are the primary reactive species in the photocatalytic process, and •O_2^- has a greater influence on the photodegradation process than h^+.

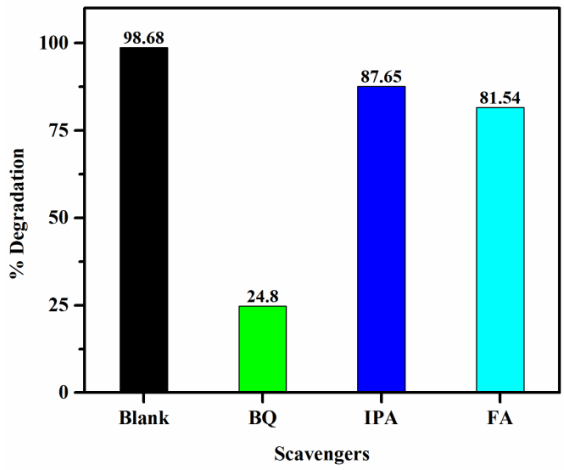

Figure 9. Scavenger effects on the performance of MB degradation over $CoFe_2O_4$-loaded g-C_3N_4 photocatalyst.

The boosted photocatalytic efficiency of the synthesized $CoFe_2O_4$-loaded g-C_3N_4 photocatalyst can be credited to the visible light sensitization of the g-C_3N_4 by the $CoFe_2O_4$ nanoparticles. To clarify the separation of electron-hole in the $CoFe_2O_4$-loaded g-C_3N_4 photocatalyst, the valence band (E_{VB}) edge and conduction band (E_{CB}) edge positions of the photocatalysts were calculated by Equations (1) and (2) [40].

$$E_{CB} = X - E - \frac{1}{2}E_g \quad (1)$$

$$E_{VB} = E_{CB} + E_g \quad (2)$$

where E_{CB} is conduction band potential, E_{VB} is valence band potential, χ is the absolute electronegativity of the photocatalyst (the χ values of g-C_3N_4 is 4.73 eV and χ values

$CoFe_2O_4$ is 5.81 eV [3,41]), E is the hydrogen scale's free electron energy, which is 4.5 eV, and E_g is band-gap energy. Hence, it was discovered that $CoFe_2O_4$ and gC_3N_4 have band-gap energies of 1.30 eV and 2.65 eV, respectively (Figure 6b,c). Then, the values of E_{VB} and E_{CB} for $CoFe_2O_4$ and g-C_3N_4 were calculated using Equations (1) and (2), respectively. The obtained results are shown in Table 2.

Table 2. Electronegativity (χ), band gap (E_g), and conduction band (E_{CB}) position and valance band (E_{VB}) of the photocatalysts on NHE.

Photocatalyst	χ (eV)	E_g (eV)	E_{CB} (eV)	E_{VB} (eV)
$CoFe_2O_4$	5.81	1.30	+0.66	+1.96
g-C_3N_4	4.73	2.65	−1.09	+1.56

Photogeneration electron-hole (e^--h^+) pairs are formed by both g-C_3N_4 and $CoFe_2O_4$ of the $CoFe_2O_4$-loaded g-C_3N_4 after irradiation by sufficient photon energy. The E_{CB} of $CoFe_2O_4$ (+0.66 eV) is less negative than that of the g-C_3N_4 (−1.09 eV), and the E_{VB} of $CoFe_2O_4$ (+1.96 eV) is more positive than the E_{VB} of g-C_3N_4 (+1.56 eV). In the case of type II heterojunction phase way, the e^- in the E_{CB} of g-C_3N_4 is transferred to the E_{CB} of $CoFe_2O_4$ and the h^+ in the E_{VB} of $CoFe_2O_4$ are transferred to E_{VB} of the g-C_3N_4. These interfacial e^--h^+ transfers suppress the charge carrier recombination and improve its photocatalytic activity. But, the e^- at E_{CB} of $CoFe_2O_4$ (+0.66 eV) cannot reduce O_2 to $\bullet O_2^-$ (E° = −0.33 eV) [16]. Alternatively, the h^+ at E_{VB} of g-C_3N_4 (+1.56 eV) has insufficient oxidation capacity to oxidize H_2O or OH^- into •OH (•OH/H_2O, E° = +1.99 eV) [16]. This contradicts the experiments on active species trapping. Clearly, the type-II photogenerated electron-hole (e^--h^+) mechanism was not appropriate for the $CoFe_2O_4$-loaded g-C_3N_4 photocatalytic system. Hence, the e^--h^+ mechanism of the $CoFe_2O_4$-loaded g-C_3N_4 may be illustrated by the direct Z-scheme system (Figure 10). In the direct Z-scheme system, the e^- in the E_{CB} of $CoFe_2O_4$ are tending to transfer and recombine with the h^+ in the E_{VB} of g-C_3N_4 by driving by the internal electric field at the intersection of surfaces, resulting in the gathering of e^- and h^+ in the E_{CB} of g-C_3N_4 and the E_{VB} of the $CoFe_2O_4$, respectively [42,43]. Consequently, the e^- in the E_{CB} of g-C_3N_4 can easily reduce the O_2 into $\bullet O_2^-$ as shown in Figure 10. Even though these h^+ in the E_{VB} of the $CoFe_2O_4$ cannot oxidize H_2O or OH^- into •OH, they can directly participate in MB pollutants adsorbed onto the surface of the $CoFe_2O_4$-loaded g-C_3N_4 photocatalyst [38]. The experiments on active species trapping are compatible with this strategy. As such, the $CoFe_2O_4$-loaded gC_3N_4 photocatalyst in the present direct Z-scheme photocatalytic system not only improves the transfer and separation efficiency of photogenerated charge carriers but also retains a high degree of redox ability during the photodegradation of MB pollutant.

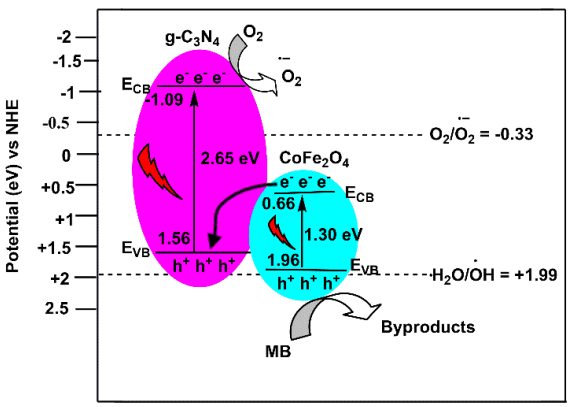

Figure 10. The $CoFe_2O_4$-loaded g-C_3N_4 under irradiation of visible-light and the proposed direct Z-scheme photocatalytic process.

3. Materials and Methods

3.1. Chemicals

Iron(III) chloride hexahydrate ($FeCl_3.6H_2O$, 97%), sodium hydroxide (NaOH, 98%), Cobalt(II) chloride hexahydrate ($CoCl_2.6H_2O$, 98%), Urea (NH_2CONH_2, 99.5%), and nitric acid (HNO_3, 70%) were obtained from Merck (India). All chemicals were utilized directly without further purification, and all experimental work was conducted with distilled water.

3.2. Synthesis of Photocatalysts

Graphitic carbon nitride (g-C_3N_4) was prepared by thermal polycondensation of urea; the detailed procedure has been described in our previously published article [7]. The $CoFe_2O_4$ loaded g-C_3N_4 photocatalyst was fabricated using the hydrothermal technique. Typically, 0.5 g of g-C_3N_4 was put in 50 mL of distilled water and sonicated for 40 min to form a uniform suspension (solution A). Similarly, 0.491g of $FeCl_3{\cdot}6H_2O$ (1.82×10^{-3} mol) and 21.62 mg of $NiCl_2{\cdot}6H_2O$ (9.1×10^{-5} mol) were put in 50 mL of distilled water and sonicated for 20 min (solution B). After that, the two solutions (solution A and solution B) were combined under sonication for 60 min. The resulting mixture was put in the Teflon-lined autoclave at 150 °C for 8 h. Then, the mixture was centrifuged and washed several times using ethanol and distilled water separately. The obtained sample was dried at 60 °C in a hot air oven to obtain the $CoFe_2O_4$ loaded g-C_3N_4 photocatalyst. Likewise, we prepared $CoFe_2O_4$-loaded g-C_3N_4 photocatalysts using the same procedure for comparison study.

3.3. Characterization Techniques

The crystallinity of the prepared samples was performed using X-ray Diffraction (D8 XRD, Bruker AXS) with Cu Kα radiation (λ = 0.154060 nm) over 2θ range of 7° to 70°. The molecular structure of the samples was examined using Fourier transform infrared spectroscopy (FT-IR, PerkinElmer–Frontier MIR/FIR) scanned in the range of 4000 to 400 cm^{-1}. The morphology and elemental composition were determined using scanning electron microscopy (SEM, JEOL- JSM 6390LV) with energy-dispersive X-ray spectroscopy (EDX, Oxford Instruments). The UV–vis diffuse reflectance (DRS) was carried out on a UV–VIS spectrophotometer (Shimadzu–UV-2450) in the range of 200–900 nm by using $BaSO_4$ as the reference. The Kubelka–Munk function (F(R) was then used to determine the optical bandgap energy of the photocatalysts. The recombination rate photoluminescence (PL) spectra were obtained by Fluorescence spectrophotometer (PerkinElmer–LS 55). By employing a BET surface area analyzer (NOVA 1000E, Quantachrom) to conduct a N_2 adsorption-desorption investigation, the BET and pore size distribution of the sample were examined. A vibrating sample magnetometer (VSM, Lakeshore-7410) was used to examine the magnetic characteristics.

3.4. Photocatalytic Experiments

To study the photocatalytic activity of the photocatalysts in the breakdown of methylene blue (MB) under irradiation of visible light, several photocatalytic experiments were carried out. To attain an equilibrium between the photocatalyst and the dye, 30 mg of photocatalyst was suspended in 100 mL of MB aqueous solution (10 mg/L) and swirled in the dark for 60 min. A 10 W LED lamp (Havells, India) was used to irradiate the photocatalytic system and a 3 mL aliquot part; these were withdrawn from the reaction solution at 20 min intervals. Then, the magnetic photocatalysts was separated using a magnet and nonmagnetic photocatalysts were separated using a centrifuge (Universal 320 Hettich). The residual concentration of MB was analyzed using a UV-visible spectrophotometer (Agilent Cary 60) at a 664 nm. The primary active species were trapped using scavengers including formic acid (FA, h^+ scavenger), benzoquinone (BQ, $\bullet O_2^-$ radical scavenger), and 2-propanol (2-PA, •OH radical scavenger).

4. Conclusions

In conclusion, we fabricated magnetically separable direct Z-scheme $CoFe_2O_4$-loaded g-C_3N_4 using a facile and simple hydrothermal technique. Characterization results confirmed that the $CoFe_2O_4$-loaded g-C_3N_4 was prepared successfully. The DRS study also showed that the absorption efficiency of the g-C_3N_4 photocatalyst was significantly extended in the visible-light region after loading nanoparticles of $CoFe_2O_4$ onto the g-C_3N_4 nanosheets. The photocatalytic performance of $CoFe_2O_4$, g-C_3N_4, and $CoFe_2O_4$-loaded g-C_3N_4 photocatalysts were examined for the MB degradation under irradiation of visible-light. The direct Z-scheme $CoFe_2O_4$-loaded g-C_3N_4 shows supreme degradation efficiency, and its activity is about 6.6 and 3.6 times higher than the $CoFe_2O_4$ and g-C_3N_4 photocatalysts, respectively. Such an extraordinary activity enhancement under irradiation of visible-light was possibly due to the significantly promoted electron-hole separation in the direct Z-scheme g-$CoFe_2O_4$-loaded g-C_3N_4; this improves the reduction/oxidation ability of the photocatalytic reaction. Mechanisms elucidated by scavenger studies revealed that $\bullet O_2^-$ and holes were the primary reactive radicals responsible for the degradation of MB. Moreover, the direct Z-scheme g-$CoFe_2O_4$-loaded g-C_3N_4 photocatalyst was collected from the aqueous solution without significant loss and demonstrated a negligible catalytic performance decline over five consecutive cycles. Therefore, this study can deliver novel insights for design and preparation of magnetic direct Z-scheme photocatalysts for dye degradation applications.

Author Contributions: The major work for this article, including conceptualization, methodology, software, validation, and writing the original draft, was performed by the first author (G.G.). The second author (M.G.) participated in conceptualization, software, and drawing. The final three authors (M.T., B.L. and W.L.) were responsible for conceptualization, supervising, and editing the article. All authors have read and agreed to the published version of the manuscript.

Funding: This research was supported by the internal grant of Addis Ababa Science and Technology University Ref. No. EG-51/11-1/20.

Data Availability Statement: Not applicable.

Acknowledgments: We acknowledge Tezpur University, Assam, India, for some characterization facility support. We are also thankful to Addis Ababa Science and Technology University, Ethiopia, for the financial support from the Internal grant project (Ref. No. EG-51/11-1/20).

Conflicts of Interest: The authors declare no conflict of interest.

References

1. Guo, X.; Ai, S.; Yang, D.; Zhao, L.; Ding, H. Synergistic photocatalytic and Fenton-like degradation of organic contaminants using peroxymonosulfate activated by $CoFe_2O_4$@g-C_3N_4 composite. *Environ. Technol.* **2021**, *42*, 2240–2253. [CrossRef] [PubMed]
2. Hassani, A.; Eghbali, P.; Ekicibil, A.; Metin, Ö. Monodisperse cobalt ferrite nanoparticles assembled on mesoporous graphitic carbon nitride ($CoFe_2O_4$/mpg-C_3N_4): A magnetically recoverable nanocomposite for the photocatalytic degradation of organic dyes. *J. Magn. Magn. Mater.* **2018**, *456*, 400–412. [CrossRef]
3. Mousavi, M.; Habibi-Yangjeh, A.; Abitorabi, M. Fabrication of novel magnetically separable nanocomposites using graphitic carbon nitride, silver phosphate and silver chloride and their applications in photocatalytic removal of different pollutants using visible-light irradiation. *J. Colloid Interface Sci.* **2016**, *480*, 218–231. [CrossRef]
4. Fujishima, A.; Honda, K. Electrochemical photolysis of water at a semiconductor electrode. *Nature* **1972**, *238*, 37–38. [CrossRef] [PubMed]
5. Yang, Y.; Luan, J. Synthesis, Property Characterization and Photocatalytic Activity of the Novel Composite Polymer Polyaniline/Bi_2SnTiO_7. *Molecules* **2012**, *17*, 2752–2772. [CrossRef] [PubMed]
6. Gebrezgiabher, M.; Gebreslassie, G.; Gebretsadik, T.; Yeabyo, G.; Elemo, F.; Bayeh, Y.; Thomas, M.; Linert, W. A C-Doped TiO_2/Fe_3O_4 Nanocomposite for Photocatalytic Dye Degradation under Natural Sunlight Irradiation. *J. Compos. Sci.* **2019**, *3*, 75. [CrossRef]
7. Gebreslassie, G.; Bharali, P.; Gebremariam, G.; Sergawie, A.; Alemayehu, E. *Graphitic Carbon Nitride with Extraordinary Photocatalytic Activity under Visible Light Irradiation*; Springer International Publishing: Cham, Switzerland, 2021; Volume 385. [CrossRef]
8. Cheng, L.; Zhang, H.; Li, X.; Fan, J.; Xiang, Q. Carbon—Graphitic Carbon Nitride Hybrids for Heterogeneous Photocatalysis. *Small* **2020**, *17*, 2005231. [CrossRef] [PubMed]
9. Wen, J.; Xie, J.; Chen, X.; Li, X. A review on g-C_3N_4-based photocatalysts. *Appl. Surf. Sci.* **2017**, *391*, 72–123. [CrossRef]

10. Zhang, M.; Yang, Y.; An, X.; Hou, L. A critical review of g-C_3N_4-based photocatalytic membrane for water purification. *Chem. Eng. J.* **2021**, *412*, 128663. [CrossRef]
11. Mishra, A.; Mehta, A.; Basu, S.; Shetti, N.P.; Reddy, K.R.; Aminabhavi, T.M. Graphitic carbon nitride (g-C_3N_4)–based metal-free photocatalysts for water splitting: A review. *Carbon* **2019**, *149*, 693–721. [CrossRef]
12. Jiang, L.; Yuan, X.; Pan, Y.; Liang, J.; Zeng, G. Doping of graphitic carbon nitride for photocatalysis: A reveiw. *Appl. Catal. B Environ.* **2017**, *217*, 388–406. [CrossRef]
13. Chebanenko, M.I.; Tikhanova, S.M.; Nevedomskiy, V.N.; Popkov, V.I. Synthesis and Structure of ZnO-Decorated Graphitic Carbon Nitride (g-C_3N_4) with Improved Photocatalytic Activity under Visible Light. *Inorganics* **2022**, *10*, 249. [CrossRef]
14. Farooq, N.; Luque, R.; Hessien, M.M.; Qureshi, A.M.; Sahiba, F.; Nazir, M.A.; ur Rehman, A. A comparative study of cerium- and ytterbium-based GO/g-C_3N_4/Fe_2O_3 composites for electrochemical and photocatalytic applications. *Appl. Sci.* **2021**, *11*, 9000. [CrossRef]
15. Ismael, M.; Wark, M. Photocatalytic activity of $CoFe_2O_4$/g-C_3N_4 nanocomposite toward degradation of different organic pollutants and their inactivity toward hydrogen production: The role of the conduction band position. *FlatChem* **2022**, *32*, 100337. [CrossRef]
16. Paul, A.; Dhar, S.S. Designing Cu2V2O7/$CoFe_2O_4$/g-C_3N_4 ternary nanocomposite: A high performance magnetically recyclable photocatalyst in the reduction of 4-nitrophenol to 4-aminophenol. *J. Solid State Chem.* **2020**, *290*, 121563. [CrossRef]
17. He, W.; Liu, L.; Ma, T.; Han, H.; Zhu, J.; Liu, Y.; Fang, Z.; Yang, Z.; Guo, K. Controllable morphology $CoFe_2O_4$/g-C_3N_4 p-n heterojunction photocatalysts with built-in electric field enhance photocatalytic performance. *Appl. Catal. B Environ.* **2022**, *306*, 121107. [CrossRef]
18. Zhang, J.; Chen, X.; Takanabe, K.; Maeda, K.; Domen, K.; Epping, J.D.; Fu, X.; Antonietti, M.; Wang, X. Synthesis of a Carbon Nitride Structure for Visible-Light Catalysis by Copolymerization. *Angew. Chem.* **2010**, *49*, 441–444. [CrossRef]
19. Gebreslassie, G.; Bharali, P.; Chandra, U.; Sergawie, A.; Boruah, P.K.; Das, M.R.; Alemayehu, E. Novel g-C_3N_4/graphene/$NiFe_2O_4$ nanocomposites as magnetically separable visible light driven photocatalysts. *J. Photochem. Photobiol. A Chem.* **2019**, *382*, 111960. [CrossRef]
20. Li, Y.; Zhou, M.; Cheng, B.; Shao, Y. Recent advances in g-C_3N_4-based heterojunction photocatalysts. *J. Mater. Sci. Technol.* **2020**, *56*, 1–17. [CrossRef]
21. Kumar, O.P.; Shahzad, K.; Nazir, M.A.; Farooq, N.; Malik, M.; Ahmad Shah, S.S.; ur Rehman, A. Photo-Fenton activated C_3N_4x/AgOy@Co1-xBi0.1-yO7 dual s-scheme heterojunction towards degradation of organic pollutants. *Opt. Mater.* **2022**, *126*, 112199. [CrossRef]
22. Wang, Q.; Li, Y.; Huang, F.; Song, S.; Ai, G.; Xin, X.; Zhao, B.; Zheng, Y.; Zhang, Z. Recent Advances in g-C_3N_4-Based Materials and Their Application in Energy and Environmental Sustainability. *Molecules* **2023**, *28*, 432. [CrossRef]
23. Gupta, N.K.; Gha, Y.; Kim, S.; Bae, J.; Kim, K.S. Photocatalytic Degradation of Organic Pollutants over MFe_2O_4 (M = Co, Ni, Cu, Zn) Nanoparticles at Neutral pH. *Sci. Rep.* **2020**, *10*, 4942. [CrossRef]
24. Nife, O.; Holinsworth, B.S.; Mazumdar, D.; Sims, H.; Sun, Q.; Yurtisigi, M.K.; Sarker, S.K.; Gupta, A.; Butler, W.H.; Musfeldt, J.L. Chemical tuning of the optical band gap in spinel ferrites: $CoFe_2O_4$ vs. $NiFe_2O_4$. *Appl. Phys. Lett.* **2013**, *103*, 082406.
25. He, H.; Lu, J. Highly photocatalytic activities of magnetically separable reduced graphene oxide-CoFe 2 O 4 hybrid nanostructures in dye photodegradation. *Sep. Purif. Technol.* **2017**, *172*, 374–381. [CrossRef]
26. Fu, Y.; Chen, H.; Sun, X.; Wang, X. Combination of cobalt ferrite and graphene: High-performance and recyclable visible-light photocatalysis. *Appl. Catal. B Environ.* **2012**, *111*, 280–287. [CrossRef]
27. Huang, S.; Xu, Y.; Xie, M.; Xu, H.; He, M.; Xia, J.; Huang, L.; Li, H. Synthesis of magnetic $CoFe_2O_4$/g-C_3N_4 composite and its enhancement of photocatalytic ability under visible-light. *Colloids Surf. A Physicochem. Eng. Asp.* **2015**, *478*, 71–80. [CrossRef]
28. Inbaraj, D.J.; Chandran, B.; Mangalaraj, C. Synthesis of $CoFe_2O_4$ and $CoFe_2O_4$/g-C_3N_4 nanocomposite via honey mediated sol-gel auto combustion method and hydrothermal method with enhanced photocatalytic and efficient Pb+2 adsorption property. *Mater. Res. Express* **2019**, *6*, 055501. [CrossRef]
29. Yuan, C.; Cao, H.; Zhu, S.; Hua, H.; Hou, L. Core-shell ZnO/$ZnFe_2O_4$@C mesoporous nanospheres with enhanced lithium storage properties towards high-performance Li-ion batteries. *J. Mater. Chem. A* **2015**, *3*, 20389–20398. [CrossRef]
30. Hou, L.; Lian, L.; Zhang, L.; Pang, G.; Yuan, C.; Zhang, X. Self-sacrifice template fabrication of hierarchical mesoporous bi-component-active ZnO/$ZnFe_2O_4$ sub-microcubes as superior anode towards high-performance lithium-ion battery. *Adv. Funct. Mater.* **2015**, *25*, 238–246. [CrossRef]
31. Dong, F.; Wu, L.; Sun, Y.; Fu, M.; Wu, Z.; Lee, S.C. Efficient synthesis of polymeric g-C 3 N 4 layered materials as novel efficient visible light driven photocatalysts. *J. Mater. Chem.* **2011**, *21*, 15171–15174. [CrossRef]
32. Liu, J.; Zhang, T.; Wang, Z.; Dawson, G.; Chen, W. Simple pyrolysis of urea into graphitic carbon nitride with recyclable adsorption and photocatalytic activity. *J. Mater. Chem.* **2011**, *21*, 14398–14401. [CrossRef]
33. Zhang, S.; Li, J.; Zeng, M.; Zhao, G.; Xu, J.; Hu, W.; Wang, X. In Situ Synthesis of Water-Soluble Magnetic Graphitic Carbon Nitride Photocatalyst and Its Synergistic Catalytic Performance. *ACS Appl. Mater. Interfaces* **2013**, *5*, 12735–12743. [CrossRef]
34. Anand, S.; Amaliya, A.P.; Janifer, M.A.; Pauline, S. Structural, morphological and dielectric studies of zirconium substituted $CoFe_2O_4$ nanoparticles. *Mod. Electron. Mater.* **2017**, *3*, 168–173. [CrossRef]
35. Sabale, S.R. Studies on catalytic activity of $MnFe_2O_4$ and $CoFe_2O_4$MNPsas mediators in hemoglobin based biosensor. *Mater. Today Proc.* **2020**, *23*, 139–146. [CrossRef]

36. Khan, M.; Pawar, H.; Kumari, M.; Patra, C.; Patel, G.; Dwivedi, U.K.; Rathore, D. Effect of concentration of SiC on physicochemical properties of $CoFe_2O_4$/SiC nanocomposites. *J. Alloys Compd.* **2020**, *840*, 155596. [CrossRef]
37. Kumar, O.P.; Ahmad, M.; Nazir, M.A.; Anum, A.; Jamshaid, M.; Shah, S.S.A.; Rehman, A. Strategic combination of metal–organic frameworks and C_3N_4 for expeditious photocatalytic degradation of dye pollutants. *Environ. Sci. Pollut. Res.* **2022**, *29*, 35300–35313. [CrossRef] [PubMed]
38. Renukadevi, S.; Jeyakumari, A.P. A one-pot microwave irradiation route to synthesis of $CoFe_2O_4$-g-C_3N_4 heterojunction catalysts for high visible light photocatalytic activity: Exploration of efficiency and stability. *Diam. Relat. Mater.* **2020**, *109*, 108012. [CrossRef]
39. Hassani, A.; Çelikdağ, G.; Eghbali, P.; Sevim, M.; Karaca, S.; Metin, Ö. Heterogeneous sono-Fenton-like process using magnetic cobalt ferrite-reduced graphene oxide ($CoFe_2O_4$-rGO) nanocomposite for the removal of organic dyes from aqueous solution. *Ultrason. Sonochem.* **2018**, *40*, 841–852. [CrossRef] [PubMed]
40. Gebreslassie, G.; Bharali, P.; Chandra, U.; Sergawie, A.; Baruah, P.K.; Das, M.R.; Alemayehu, E. Hydrothermal Synthesis of g-C_3N_4/$NiFe_2O_4$ Nanocomposite and Its Enhanced Photocatalytic Activity. *Appl. Organomet. Chem.* **2019**, *33*, e5002. [CrossRef]
41. Hafeez, H.Y.; Lakhera, S.K.; Narayanan, N.; Harish, S.; Hayakawa, Y.; Lee, B.K.; Neppolian, B. Environmentally Sustainable Synthesis of a $CoFe_2O_4$-TiO_2/rGO Ternary Photocatalyst: A Highly Efficient and Stable Photocatalyst for High Production of Hydrogen (Solar Fuel). *ACS Omega* **2019**, *4*, 880–891. [CrossRef]
42. Xu, Q.; Zhang, L.; Yu, J.; Wageh, S.; Al-Ghamdi, A.A.; Jaroniec, M. Direct Z-scheme photocatalysts: Principles, synthesis, and applications. *Mater. Today* **2018**, *21*, 1042–1063. [CrossRef]
43. Low, J.; Yu, J.; Jaroniec, M.; Wageh, S.; Al-Ghamdi, A.A. Heterojunction Photocatalysts. *Adv. Mater.* **2017**, *29*, 1601694. [CrossRef] [PubMed]